

Spectral Coherence Index: A Model-Free Metric for Protein Structural Ensemble Quality Assessment

Yuda Bi, Huaiwen Zhang, Jingnan Sun, and Vince D. Calhoun, *Fellow, IEEE*

Abstract—Protein structural ensembles from NMR spectroscopy capture biologically important conformational heterogeneity, but it remains difficult to determine whether observed variation reflects coordinated motion or noise-like artifacts. We evaluate the Spectral Coherence Index (SCI), a model-free, rotation-invariant summary derived from the participation-ratio effective rank of the inter-model pairwise distance-variance matrix. Under grouped primary analysis of a Main110 cohort of 110 NMR ensembles (30–403 residues; 10–30 models per entry), SCI separated experimental ensembles from matched synthetic incoherent controls with AUC-ROC = 0.973 and Cliff’s $\delta = -0.945$. Relative to an internal 27-protein pilot, discrimination softened modestly, showing that pilot-era thresholds do not transfer perfectly to a larger, more heterogeneous cohort: the primary operating point $\tau = 0.811$ yielded 95.5% sensitivity and 89.1% specificity. PDB-level sensitivity remained nearly unchanged (AUC = 0.972), and an independent 11-protein holdout reached AUC = 0.983. Across 5-fold grouped stratified cross-validation and leave-one-function-class-out testing, SCI remained strong (AUC = 0.968 and 0.971), although σ_{R_g} was the stronger single-feature discriminator and a QC-augmented multifeature model generalized best (AUC = 0.989 and 0.990). Residue-level validation linked SCI-derived contributions to experimental RMSF across 110 proteins and showed broad concordance with GNM-based flexibility patterns. Rescue analyses showed that Main110 softening arose mainly from size and ensemble normalization rather than from loss of spectral signal. Together, these results establish SCI as an interpretable, bounded coherence summary that is most useful when embedded in a multimetric QC workflow for heterogeneous protein ensembles.

Index Terms—conformational diversity, effective rank, NMR, spectral coherence, structural ensemble, AlphaFold

I. INTRODUCTION

PROTEINS are not static entities. Their biological function—including catalysis, signal transduction, and molecular recognition—depends critically on conformational dynamics spanning timescales from picoseconds to seconds [1], [2]. Nuclear magnetic resonance (NMR) spectroscopy remains a primary experimental technique for char-

acterizing this heterogeneity at atomic resolution, producing multi-model structural ensembles that represent conformations accessible to a protein in solution [3]–[5]. In parallel, modern deep-learning predictors achieve remarkable accuracy for single-structure modeling, and recent efforts extend these models toward sampling multiple conformations [6]–[10], [47]. Despite this progress, a fundamental gap persists: there is no widely adopted, model-free metric that quantifies *how coherently* an ensemble’s structural variation is organized—i.e., whether inter-residue distance changes are concentrated into a few coordinated modes or instead appear as diffuse, noise-like fluctuations.

Several metrics characterize ensemble diversity, each with notable limitations. Pairwise RMSD requires structural superposition and yields a distribution rather than a single ensemble-level summary [11], [12]. Global measures such as the radius-of-gyration standard deviation (σ_{R_g}) miss local rearrangements or hinge-like motions that preserve overall size [13]. PCA-based variance ratios depend on coordinate alignment and can be sensitive to the chosen reference [14], [15], while contact- or clustering-based summaries introduce arbitrary cutoffs or thresholds that can yield discontinuous behavior [16], [17]. These limitations motivate a metric that (i) operates directly on inter-residue distances to avoid superposition artifacts; (ii) summarizes the spectral organization of distance variation rather than relying on a single dominant component; and (iii) produces a single interpretable value on [0, 1].

Spectral methods have a long history in structural biology. Elastic network models such as the Gaussian Network Model (GNM) [18], [19] and the Anisotropic Network Model (ANM) [20] use the eigenspectrum of a connectivity Laplacian or Hessian to predict collective motions from a single structure. The concept of effective rank—quantifying the effective dimensionality of a spectrum via the participation ratio [22] or spectral entropy [21], [23]—is widely used in signal processing and random matrix theory to summarize spectral concentration versus dispersion. Scheurer et al. [23] applied spectral entropy to coordinate-covariance eigenspectra to assess *sampling completeness* in molecular dynamics trajectories. In molecular dynamics more broadly, quasi-harmonic analysis and principal component analysis of trajectories [14], [24], [25] decompose conformational fluctuations into modes, but they operate on superposed Cartesian coordinates and therefore depend on alignment and reference choices. To our knowledge, no effective-rank measure has previously been applied to the pairwise *distance-variance matrix* of a structural ensemble as a coherence diagnostic. Because the distance-

Manuscript received XXXX XX, 2026.

Y. Bi is with the Tri-institutional Center for Translational Research in Neuroimaging and Data Science (TReNDS), Georgia State University, Georgia Institute of Technology, and Emory University, Atlanta, GA 30303 USA (e-mail: ybi3@gsu.edu).

H. Zhang is with the School of Computer Science and Technology, Xidian University, Xi’an 710126, China.

J. Sun is with the Departments of Biomedical Engineering, Johns Hopkins University, Baltimore, MD 21287 USA.

V. D. Calhoun is with the Tri-institutional Center for Translational Research in Neuroimaging and Data Science (TReNDS), Georgia State University, Georgia Institute of Technology, and Emory University, Atlanta, GA 30303 USA, and also with the School of Electrical and Computer Engineering, Georgia Institute of Technology, Atlanta, GA 30332 USA (e-mail: vcalhoun@gsu.edu).

variance matrix captures inter-residue coordination rather than coordinate-space spread, such a measure is complementary to—not a surrogate for—coordinate-covariance spectral entropy.

In this work, we evaluate the Spectral Coherence Index (SCI), a model-free, rotation-invariant metric derived from the participation ratio effective rank of the inter-model pairwise distance-variance matrix, in an expanded Main110 validation setting designed not to redefine the metric, but to test whether its coherence signal survives broader biological heterogeneity and stricter validation regimes than our earlier internal 27-protein pilot could support. The main contributions are:

- 1) **Expanded validation beyond the internal pilot.** We scale from an internal 27-protein pilot to a canonical Main110 cohort of 110 NMR ensembles plus a fixed 11-protein holdout, showing that the SCI signal survives broader cohort heterogeneity while also revealing softer specificity and threshold non-transferability that were not visible at pilot scale.
- 2) **Canonical metric and grouped inference layer.** We retain the canonical definition $SCI = 1 - r_{\text{eff}}/d$, where r_{eff} is the participation ratio of the positive eigenvalue spectrum of the distance-variance matrix and $d = \min(L, M-1)$ normalizes degrees of freedom (L : number of residues; M : number of models). We establish grouped UniProt or analysis-group inference as the primary paper layer, with PDB-level analysis reported as a sensitivity check.
- 3) **Benchmarking, generalization, and normalization analysis.** We compare SCI with σ_{R_g} , $SCI+\sigma_{R_g}$, PCA variance ratio, contact density, and a QC-augmented multifeature model under 5-fold grouped cross-validation, leave-one-function-class-out validation, and independent holdout testing. We further show that raw spectral quantities (r_{eff} , top-1 energy fraction, top-3 energy fraction) and calibrated SCI models augmented with residue count and model count nearly recover the lost discrimination, explaining why Main110 is harder than the pilot.
- 4) **Residue-level biological validation.** We validate SCI-derived residue contributions against experimental RMSF and Gaussian network model predictions across 110 proteins, including paired statistical comparison and outlier analysis, and we treat allosteric, apo/olo, and intrinsically disordered examples as contextual case studies.
- 5) **Practical multimetric QC guidance.** We show that coherence (SCI), amplitude (σ_{R_g}), and eigenvector smoothness are complementary diagnostics. Function-class breakdowns, threshold error analyses, ensemble-size sensitivity, and synthetic failure-mode stress tests support their combined use, while making clear that fixed QC thresholds should be interpreted as screening heuristics rather than universal pass/fail rules.

The remainder of this paper is organized as follows. Section II reviews related work on protein ensemble analysis and spectral methods. Section III describes the dataset, the

SCI formulation, baseline metrics, and statistical procedures. Section IV presents the main experimental results. Section V discusses methodological implications, limitations, and practical guidance. Section VI concludes.

II. RELATED WORK

A. Protein Ensembles: Experiment, Prediction, and Quality

The energy landscape theory established that proteins exist as statistical ensembles of conformational states [2], [33], with allosteric regulation, catalysis, and molecular recognition depending on coordinated structural fluctuations [1], [34], [35]. NMR spectroscopy provides direct experimental access to these ensembles through multi-model PDB depositions [3]–[5], capturing coherent motions such as hinge bending and domain closure [36], [37]. On the computational side, AlphaFold2 [6], RoseTTAFold [7], ESMFold [8], and protein language models [26] have achieved high single-structure accuracy, spurring ensemble extensions via sequence subsampling [47], stochastic sampling [9], diffusion models [10], and trainable reimplementations [27]. Molecular dynamics remains the physics-based gold standard for conformational sampling [28], [29] but is computationally expensive. This proliferation of ensemble sources creates an urgent need for quality metrics that assess whether the resulting variation is structurally coherent or merely noise-like. Existing geometric metrics—pairwise RMSD [11], [12], radius of gyration statistics [13], and contact map variability [16]—each have well-known limitations (Section I). Statistical approaches such as structure clustering [17], backbone entropy [30], TM-score [31], and ensemble validation tools (PSVS [32], wwPDB-NMR [5]) focus on restraint satisfaction or single-structure quality rather than spectral organization of conformational variation.

B. Spectral Methods and Effective Rank

Spectral decomposition has a rich history in structural biology. The Gaussian Network Model [18], [19] and the Anisotropic Network Model [20] decompose connectivity matrices into normal modes, predicting B-factors [38], identifying functional sites [39], and revealing allosteric pathways [40]. Quasi-harmonic analysis [24] and essential dynamics [14], [15], [25] apply PCA to Cartesian trajectories but require structural superposition, introducing rotation-frame artifacts. Distance-based representations such as multidimensional scaling [41] avoid this limitation. Scheurer et al. [23] applied spectral entropy—the Shannon-entropy effective rank of coordinate-covariance eigenspectra—to assess *sampling completeness* in molecular dynamics trajectories. The participation ratio, originally introduced to characterize eigenstate localization [42], quantifies how many components of a distribution contribute meaningfully: for a normalized spectrum $\{\tau_k\}$, $r_{\text{eff}} = 1/\sum_k \tau_k^2$ equals 1 when all weight is on a single component and equals the number of components n^+ when weight is uniform. Roy and Vetterli [21] formalized effective rank using Shannon entropy of singular values; the participation ratio is a mathematically related alternative [22], and in practice the two formulas produce

near-identical rankings (Section IV-C, $r > 0.95$). The key distinction between SCI and prior spectral-entropy approaches therefore lies not in the effective-rank formula but in the *input representation*: the pairwise distance-variance matrix. This makes SCI rotation-invariant and diagnostic of inter-residue coordination, whereas coordinate-covariance spectral entropy measures sampling breadth.

C. Ensemble Quality in Biomedical Informatics

Structural ensemble quality has direct implications for downstream health informatics tasks. Ensemble docking methods for binding-site prediction [43] can propagate artifacts from incoherent ensembles. Epitope mapping leveraging conformational diversity [44] and variant effect prediction tools incorporating structural dynamics [45] both depend on ensemble quality as a prerequisite for reliable inference. More broadly, automated quality gates for structural data—analogue to QC metrics in genomics pipelines [46]—are essential for maintaining reproducibility in computational analyses that inform clinical decision-making.

III. METHODS

A. Dataset Construction

1) *Expanded Main110 Cohort*: We promoted an expanded cohort of $N = 110$ NMR multi-model protein structures from a 125-candidate screen of PDB NMR entries, requiring usable $C\alpha$ coordinates, successful preprocessing, and resolved metadata after UniProt-mapping quality control. Four non-holdout candidates were excluded because of unresolved mapping or hard QC failures, and one mapped unresolved case (6LF5) was retained as a PDB-level fallback analysis group. The final main cohort spans proteins of 30–403 residues with 10–30 models per entry (median $M = 20$) across 11 broad function classes. $C\alpha$ coordinates were extracted from mmCIF files using Biotite.

2) *Independent Holdout*: An additional 11 NMR proteins were reserved as a fixed independent holdout and were not used to define the canonical main-cohort summary statistics or grouped cross-validation models. The holdout spans 27–75 residues with 10–25 models per entry (median $M = 20$) and is used as an external NMR-vs-synthetic-incoherent-control validation set.

3) *Synthetic Incoherent Controls*: As a negative control representing ensembles with incoherent structural variation, we generated synthetic incoherent controls by perturbing the first NMR conformer along $K = 2$ randomly sampled global deformation modes. Specifically, for each protein with reference coordinates $\mathbf{x}_0 \in \mathbb{R}^{3L}$, the m -th synthetic model is

$$\mathbf{x}_m = \mathbf{x}_0 + \sum_{k=1}^K \alpha_{mk} \mathbf{v}_k, \quad (1)$$

where $\{\mathbf{v}_k\}_{k=1}^K$ are orthonormal vectors in \mathbb{R}^{3L} obtained by Gram–Schmidt orthogonalization of standard Gaussian random vectors, and $\alpha_{mk} \sim \mathcal{N}(0, \sigma^2)$ with $\sigma = 0.2 \text{ \AA}$ (chosen to match the order of magnitude of NMR $C\alpha$ coordinate variation; see Section III-D6 for a discussion of perturbation

magnitudes). $K = 2$ modes ensure that the control is low-rank yet minimally coherent in distance-variance space; higher K would produce a more diffuse control (tested as a separate failure mode with $K = 10$). Each synthetic ensemble has the same number of models M as the corresponding NMR ensemble in both the main and holdout splits. Although the perturbation is low-rank in coordinate space ($K = 2$), the resulting patterns in distance variance space are typically more diffuse due to the nonlinear distance mapping (see Section IV).

4) *AlphaFold Single-Structure Reference*: As a reference-only third group, we obtained AlphaFold2-predicted structures for 40 proteins in the main cohort with resolved mappings and usable AlphaFold coverage from the AlphaFold Protein Structure Database [6]. Each prediction provides a single model ($M = 1$), precluding ensemble-based SCI computation. We therefore employ a single-structure spectral proxy (Section III-B5). Per-residue confidence scores (pLDDT) were extracted from B-factor fields. Sequence matching required a protein-level metadata mapping and compatible chain coverage; these AlphaFold results are reported only as a reference analysis and are not directly comparable to the ensemble-based SCI values.

Figure 1 summarizes the SCI workflow from ensemble input through spectral compression to multimetric QC interpretation.

B. Spectral Coherence Index (SCI)

Throughout this study, we define the positive class as NMR ensembles and use SCI directly as the classification score: higher SCI indicates more coherent variation, corresponding to the NMR ensemble class.

1) *Distance Variance Matrix*: Consider a structural ensemble with L residues per model and M conformers. For the m -th model, define the pairwise $C\alpha$ – $C\alpha$ distance matrix

$$D_m(i, j) = \|\mathbf{r}_m^{(i)} - \mathbf{r}_m^{(j)}\|_2, \quad 1 \leq i, j \leq L, \quad (2)$$

where $\mathbf{r}_m^{(i)} \in \mathbb{R}^3$ is the coordinate of the i -th $C\alpha$ atom in model m . The *distance-variance matrix* $V \in \mathbb{R}^{L \times L}$ is defined entry-wise as

$$V(i, j) = \text{Var}_m[D_m(i, j)] = \frac{1}{M} \sum_{m=1}^M (D_m(i, j) - \bar{D}(i, j))^2, \quad (3)$$

where $\bar{D}(i, j) = \frac{1}{M} \sum_{m=1}^M D_m(i, j)$ is the mean distance. We use the population variance ($1/M$); using the sample variance ($1/(M-1)$) would yield an identical SCI, since the constant factor cancels in the normalized spectrum τ_k . Each entry $V(i, j) \geq 0$ is the scalar variance of the (i, j) pairwise distance across M models.

Several properties of V are important:

- V is symmetric with non-negative entries, but is *not* guaranteed positive semi-definite (PSD). It is an entry-wise variance map, not a covariance matrix in the sense of $\text{Cov}(\text{vec}(D), \text{vec}(D)^\top)$.
- The diagonal entries satisfy $V(i, i) = \text{Var}_m[D_m(i, i)] = \text{Var}_m[0] = 0$ for all i , since self-distances are identically zero. Therefore $\text{tr}(V) = \sum_i V(i, i) = 0$, which implies $\sum_k \lambda_k = 0$: the positive and negative eigenvalue masses

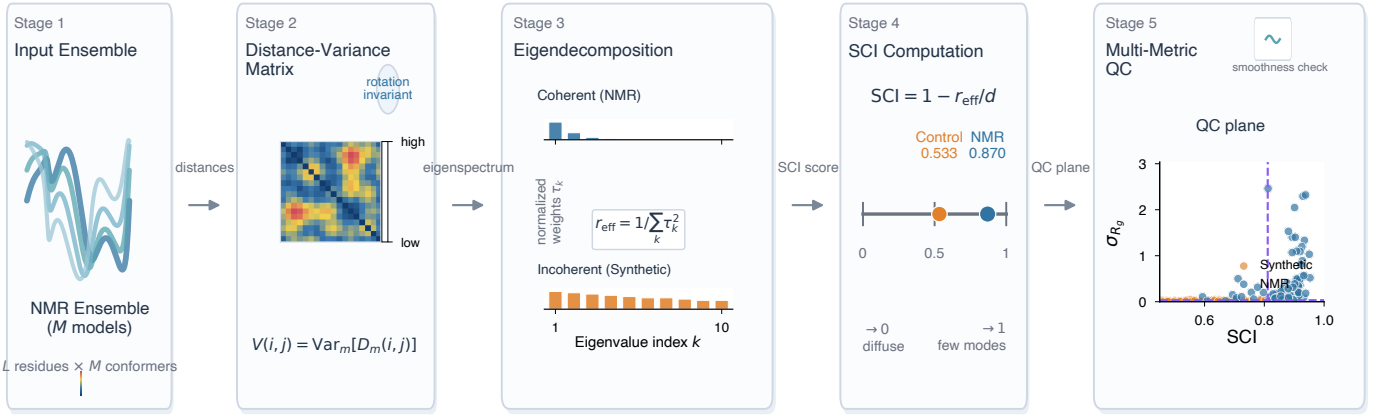


Fig. 1. Conceptual overview of the SCI workflow. Starting from an NMR ensemble of M conformers, pairwise distance variation is summarized in the distance-variance matrix V , eigendecomposed to obtain the normalized positive-spectrum weights τ_k , compressed into the bounded score $\text{SCI} = 1 - r_{\text{eff}}/d$, and finally interpreted jointly with σ_{R_g} in a multimetric QC plane. The SCI anchors shown in Stage 4 correspond to the current Main110 mean SCI for NMR ensembles (0.870) and matched synthetic incoherent controls (0.533), and the QC plane in Stage 5 uses the current Main110 data with the manuscript’s screening thresholds.

are exactly equal. The retained positive-spectrum fraction is thus 0.50 for every ensemble—a structural identity, not a numerical artifact.

- Because $D_m(i, j)$ depends only on inter-atomic distances, V is *rotation-invariant*: no structural superposition or reference frame is required.
- Although V is not PSD, its positive eigenspectrum provides a compact summary of coordinated variance patterns across residue pairs. We define SCI on the positive part of the spectrum only; negative eigenvalues are discarded. The fraction of retained spectral mass is reported in the project outputs as a transparency diagnostic.

2) *Eigendecomposition and Normalized Spectrum*: Let $\lambda_1 \geq \lambda_2 \geq \dots \geq \lambda_L$ be the eigenvalues of V . Since V is not PSD, some λ_k may be negative. We retain only the positive eigenvalues exceeding a numerical threshold $\varepsilon = 10^{-10}$:

$$\Lambda^+ = \{\lambda_k : \lambda_k > \varepsilon\}, \quad n^+ = |\Lambda^+|. \quad (4)$$

Denote the filtered eigenvalues as $\lambda_1^+ \geq \dots \geq \lambda_{n^+}^+$. The normalized spectrum is

$$\tau_k = \frac{\lambda_k^+}{n^+}, \quad k = 1, \dots, n^+, \quad (5)$$

$$\sum_{j=1}^{n^+} \lambda_j^+$$

satisfying $\tau_k \geq 0$ and $\sum_k \tau_k = 1$, forming a discrete probability distribution over variance modes.

3) *Effective Rank via Participation Ratio*: The participation ratio effective rank [21], [22] of the normalized spectrum is

$$r_{\text{eff}} = \frac{(\sum_k \tau_k)^2}{\sum_k \tau_k^2} = \frac{1}{\sum_k \tau_k^2}. \quad (6)$$

This quantity has the following extremal behavior:

- $r_{\text{eff}} = 1$ when all variance is concentrated in a single mode ($\tau_1 = 1$);
- $r_{\text{eff}} = n^+$ when variance is uniformly distributed ($\tau_k = 1/n^+$ for all k).

Thus r_{eff} can be interpreted as the effective number of independent variation modes.

4) *SCI Definition*: The Spectral Coherence Index is defined as

$$\text{SCI} = 1 - \frac{r_{\text{eff}}}{d}, \quad d = \min(L, M-1). \quad (7)$$

The normalization constant $d = \min(L, M-1)$ serves as an effective degrees-of-freedom scale. The $M-1$ term reflects the fact that M ensemble members yield $M-1$ independent deviations from the mean, analogous to the degrees-of-freedom correction in sample variance. We note that V is not a sample covariance matrix *sensu stricto*, so $M-1$ is not a strict rank upper bound: empirically, n^+ (mean ≈ 43 for $L \approx 90$, $M \approx 20$) exceeds $M-1$ because the entry-wise variance map is not generated by a rank- $(M-1)$ process. However, $\min(L, M-1)$ empirically yields $\text{SCI} \in [0, 1]$ for all ensembles in our dataset and scales appropriately with both protein size and ensemble size; the bound is not a mathematical guarantee, since a perfectly uniform positive spectrum could in principle produce $r_{\text{eff}} > d$. Empirical validation in the project outputs confirms that all r_{eff} values fall well below d .

SCI has the following interpretation:

- $\text{SCI} \rightarrow 1$: the spectrum is highly concentrated; distance variation across models is dominated by few coherent modes, consistent with coordinated structural deformations (e.g., hinge bending, domain closure).
- $\text{SCI} \rightarrow 0$: the spectrum is diffuse; distance variation is spread across many modes, indicating incoherent, noise-like fluctuations.

Crucially, SCI measures the *coherence* of variation—the degree to which pairwise distance changes are coordinated across residue pairs—not its magnitude.

SCI belongs to the broader family of effective-rank measures, which includes the Shannon-entropy variant used by Scheurer et al. [23] to assess conformational sampling completeness from coordinate-covariance eigenspectra. The choice of participation ratio versus Shannon entropy is a minor technical detail: both yield near-identical SCI values (Section IV-C, $r > 0.95$). The substantive distinction is the

input representation: SCI summarizes the eigenspectrum of the distance-variance matrix V , making it rotation-invariant and diagnostic of inter-residue coordination, whereas spectral entropy of coordinate covariance quantifies how broadly conformational space has been explored. The two measures answer complementary questions about ensemble quality.

We additionally define the *spectral dispersion index* $DI = 1 - \text{SCI} = r_{\text{eff}}/d$, which increases with spectral diffuseness. Higher DI does not imply greater conformational diversity; it indicates that distance changes across models lack coordinated structure.

5) *Single-Structure Spectral Proxy*: For AlphaFold single structures ($M = 1$), the distance-variance matrix is identically zero. As an alternative, we compute a spectral proxy from the double-centered Gram matrix of the pairwise distance matrix [41]:

$$B = -\frac{1}{2} H D^{\circ 2} H, \quad H = I_L - \frac{1}{L} \mathbf{1}_L \mathbf{1}_L^\top, \quad (8)$$

where $D^{\circ 2}$ denotes the element-wise squared distance matrix and H is the centering matrix. The SCI formula (6)–(7) is then applied to B with $d = L$. This proxy measures intrinsic fold geometry spectral concentration rather than cross-model variation coherence, and is *not* directly comparable to the ensemble-based SCI ($d = \min(L, M-1)$). All cross-group comparisons involving AlphaFold are therefore interpretive.

C. Baseline Metrics

To contextualize SCI, we compare it against three baseline metrics computable from the same $C\alpha$ ensembles:

- 1) **Radius of gyration standard deviation** (σ_{R_g}): the standard deviation of the radius of gyration across ensemble members, where $R_g(S_m) = \sqrt{\frac{1}{L} \sum_{i=1}^L \|\mathbf{r}_m^{(i)} - \bar{\mathbf{r}}_m\|^2}$ and $\bar{\mathbf{r}}_m$ is the centroid of model m . This captures global size fluctuations but is insensitive to local conformational changes.
- 2) **PCA variance ratio** ($\lambda_1^{\text{PCA}}/\Sigma$): the fraction of total variance explained by the first principal component, computed from the $3L$ -dimensional superposed coordinate vectors. This requires structural alignment and is sensitive to reference frame choice.
- 3) **Contact density**: the mean number of $C\alpha$ – $C\alpha$ contacts per residue (threshold 8 Å), averaged across models. This metric is not expected to discriminate NMR from synthetic controls and serves as a negative baseline.

D. Statistical Analysis

All primary discrimination analyses treat experimental NMR ensembles as the positive class and matched synthetic incoherent controls as the negative class.

1) *Primary and Sensitivity Analyses*: The canonical manuscript endpoint is a grouped main-cohort comparison in which NMR and matched synthetic incoherent controls are paired by UniProt-derived analysis group. The main cohort contains 110 analysis groups: 109 resolved UniProt groups and one retained PDB-level fallback (6LF5). We report AUC-ROC, Cliff’s delta, paired permutation tests, and bootstrap

confidence intervals for the mean paired SCI difference. A PDB-level analysis on the same 110 proteins is reported as a sensitivity check, and the fixed 11-protein holdout is evaluated independently as an external NMR-vs-synthetic-incoherent-control test set. Legacy27 results are retained only as historical context and not as a separate inferential cohort.

2) *Reference Comparison and Thresholding*: For the reference-only AlphaFold analysis, a Kruskal–Wallis test assesses differences across three groups (NMR, synthetic incoherent controls, and AlphaFold proxy), followed by pairwise Mann–Whitney U tests with multiple-comparison correction. Because the AlphaFold proxy uses the single-structure Gram-matrix formulation of Section III-B5, these comparisons are interpretive rather than directly comparable to the ensemble-based SCI results. We estimate operating thresholds with Youden’s J and summarize threshold uncertainty by bootstrap confidence intervals.

3) *Generalization Analyses*: Generalization is evaluated at three levels. First, all manuscript results use 5-fold grouped cross-validation with `StratifiedGroupKFold(n_splits=5, shuffle=True, random_state=42)`, grouping by `analysis_group_id` and stratifying by the binary NMR/control label. The code retains `GroupKFold` as a backward-compatible fallback for older environments, but it was not used in the reported results. This preserves paired NMR/control samples within analysis-group splits on the main cohort. Second, leave-one-function-class-out validation tests transfer across the 11 annotated protein function classes. Third, the independent holdout is scored using models fitted on the main cohort only. These analyses are reported for SCI, σ_{R_g} , $\text{SCI} + \sigma_{R_g}$, and a QC-full model that combines SCI, σ_{R_g} , PCA variance ratio, and top-eigenvector smoothness. To investigate why SCI softens on Main110, we repeat the same grouped-CV, leave-one-function-class-out, and holdout regimes for raw spectral quantities (r_{eff} , top-1 energy fraction, top-3 energy fraction) and for calibrated SCI models that add residue count and/or model count as covariates.

4) *Biological Validation*: We summarize three biological validation layers. At the residue level, Spearman correlations compare SCI-derived residue contributions with experimental RMSF and with GNM-predicted RMSF, and paired Wilcoxon tests compare these two per-protein correlation distributions. We additionally report negative and weak-correlation outliers. At the protein level, we evaluate curated allosteric and apo/holo pairs to determine whether SCI tracks coherence differently from amplitude-sensitive metrics, but we interpret these small-sample analyses as contextual case studies rather than formal validation. Finally, available intrinsically disordered proteins are summarized separately as high-flexibility examples.

5) *Eigenvector Smoothness Score*: Let \mathbf{u}_1 denote the top eigenvector of the distance-variance matrix V . To assess whether this dominant mode respects the protein’s chain topology, we define a smoothness score via the Rayleigh quotient on the sequential residue graph Laplacian \mathcal{L} . The graph is the path graph on L residues (adjacency $A_{i,i+1} = 1$), and $\mathcal{L} = D_{\text{deg}} - A$ is the combinatorial Laplacian. We compute

$E = \mathbf{u}_1^\top \mathcal{L} \mathbf{u}_1 / \mathbf{u}_1^\top \mathbf{u}_1$ and define smoothness $= 1/(1 + E) \in [0, 1]$, where values near 1 indicate that the dominant mode varies slowly along the chain (spatially coherent), and lower values indicate rapid residue-to-residue sign changes (spatially incoherent).

6) *Robustness and Failure-Mode Diagnostics*: To stress-test the multimetric QC framework, we generate four synthetic failure types from the reference NMR ensembles used by the QC stress-test pipeline:

- 1) **i.i.d. Gaussian noise**. Per-atom i.i.d. perturbations $\mathcal{N}(0, 0.2^2)$ Å are added independently to each coordinate of each model.
- 2) **Generator mode collapse**. Three conformations are drawn uniformly at random from the NMR ensemble and replicated to fill M models, with per-atom jitter $\mathcal{N}(0, 0.01^2)$ Å added to each copy.
- 3) **Residue shuffle**. Each residue in each model receives an independent random displacement of magnitude $|\mathcal{N}(0, 0.2)|$ Å in a uniformly random direction, destroying spatial correlation between neighboring residues.
- 4) **High-rank perturbation** ($K = 10$). Ten randomly sampled global deformation modes with $\sigma = 0.1$ Å are applied (using Eq. (1) with $K = 10$), producing spectrally diffuse variation.

The perturbation magnitudes ($\sigma = 0.2$ Å for i.i.d. and shuffle, $\sigma = 0.1$ Å for high-rank) are chosen to match the order of magnitude of coordinate-level NMR ensemble variation (typical $C\alpha$ RMSD ≈ 0.5 – 2.0 Å) while keeping the artifacts subtle enough that naive metrics may miss them. The $K = 2$ baseline control (Section III-A) uses the same low-rank perturbation scheme but with fewer modes, producing a clear coherence deficit.

IV. RESULTS

A. SCI Distinguishes NMR Ensembles from Synthetic Incoherent Controls

The grouped primary Main110 analysis shows a clear separation between experimental NMR ensembles and matched synthetic incoherent controls. Mean SCI was 0.870 ± 0.068 for NMR versus 0.533 ± 0.209 for the matched synthetic incoherent controls, with a mean paired difference of 0.337 (95% bootstrap CI: $[0.305, 0.370]$) and paired permutation $p < 10^{-4}$. The effect size remained very large (Cliff’s $\delta = -0.945$), indicating that higher SCI is strongly associated with the experimental ensemble class. Using SCI directly as the score yielded grouped AUC-ROC $= 0.9726$ (Fig. 2c). The Youden- J operating point was $\tau = 0.811$, corresponding to 95.5% sensitivity and 89.1% specificity; the bootstrap confidence interval for the threshold was $[0.686, 0.814]$.

The grouped result is the manuscript’s primary inferential layer because the expanded cohort is analyzed at the resolved UniProt or analysis-group level rather than by counting every archival entry as an independent biological target. In the canonical Main110 set, 109 groups map cleanly to UniProt identifiers and one group is retained through the fallback identifier PDB:6LF5; this bookkeeping avoids pseudo-replication without discarding a structurally valid ensemble.

The same conclusion persisted in the two confirmatory layers used in this manuscript. A PDB-level sensitivity analysis remained nearly unchanged (AUC $= 0.9716$, Cliff’s $\delta = -0.943$, $\tau = 0.813$), showing that the coherence signal is not created by the grouping rule. The fixed 11-protein holdout also preserved strong separation, with mean SCI 0.9068 ± 0.0290 for NMR versus 0.7354 ± 0.0865 for matched synthetic incoherent controls, AUC $= 0.9835$, and a descriptive holdout threshold $\tau = 0.866$ achieving 100% sensitivity and 90.9% specificity. The holdout controls are therefore more challenging than the main synthetic incoherent controls in absolute SCI, yet the ranking signal remains robust.

Relative to the internal 27-protein pilot rerun, however, the expanded benchmark is modestly but meaningfully harder. The pilot achieved AUC $= 0.9877$, Cliff’s $\delta = -0.9753$, and a Youden threshold $\tau = 0.8249$ with 100% sensitivity and 92.6% specificity. Main110 therefore reduces AUC by 0.0151 and specificity by 3.5 percentage points while retaining strong sensitivity. This softening is informative rather than discouraging: the broader cohort spans 11 function classes and a wider range of residue counts and model counts, exposing heterogeneity that the pilot could not resolve.

Error analysis makes the failure pattern explicit. At the grouped threshold, 12 of 110 NMR groups fall below τ and 6 of 110 synthetic incoherent controls rise above it. These cases are not evenly distributed. Low-model ensembles ($M \leq 10$) represent only 11 of 110 groups (10.0%) but account for 10 of the 12 NMR misses (83.3%), an approximately 8.3-fold enrichment. Short proteins ($L \leq 50$) represent 13 of 110 groups (11.8%) but account for 5 of the 6 control overcalls (83.3%), an approximately 7.1-fold enrichment. Thus Main110 reveals two distinct SCI stress points: NMR misses are disproportionately concentrated among low-model ensembles, whereas control overcalls are enriched among very short proteins.

Function-class summaries reinforce the same interpretation (Table III). By mean SCI, chaperone, other, toxin, enzyme, and transport proteins are the weakest classes, and the viral split is the hardest leave-one-function-class-out transfer setting for SCI (AUC $= 0.906$). In contrast, σ_{R_g} remains at or above 0.938 AUC on every held-out function class. Representative low-margin and threshold-failed groups are listed in Table IV.

B. Reference Analysis: AlphaFold Single-Structure Proxy

The AlphaFold comparison remains methodologically separate from the main ensemble analysis. Because each AlphaFold prediction comprises a single model, SCI is computed via the Gram-matrix proxy of Section III-B5, which summarizes intrinsic fold-geometry concentration rather than cross-model coherence. The proxy therefore serves as a reference analysis, not as a directly comparable third arm of the primary discrimination task. The AlphaFold proxy values were high (0.9813 ± 0.0155 for 40 matched structures), a Kruskal-Wallis test across NMR, synthetic incoherent controls, and AlphaFold proxies remained highly significant ($H = 205.52$, $p = 2.36 \times 10^{-45}$), and all pairwise comparisons survived correction. However, the proxy showed only a weak, non-significant association with mean pLDDT (Spearman $\rho =$

TABLE I
EXPANDED COHORT SUMMARY USED IN THIS MANUSCRIPT. THE GROUPED PRIMARY ENDPOINT COMPRISES 110 ANALYSIS GROUPS: 109 UNIPROT-MAPPED GROUPS AND ONE RETAINED PDB-LEVEL FALLBACK GROUP.

Cohort	Role	n	Residues	Models per entry
Main110 NMR	grouped primary and PDB sensitivity	110	30–403	10–30 (median 20)
Holdout NMR	independent external validation	11	27–75	10–25 (median 20)
AlphaFold proxy	reference-only single-structure analysis	40	matched main-cohort subset	1
Excluded candidates	unresolved mapping or hard QC failure	4	—	—

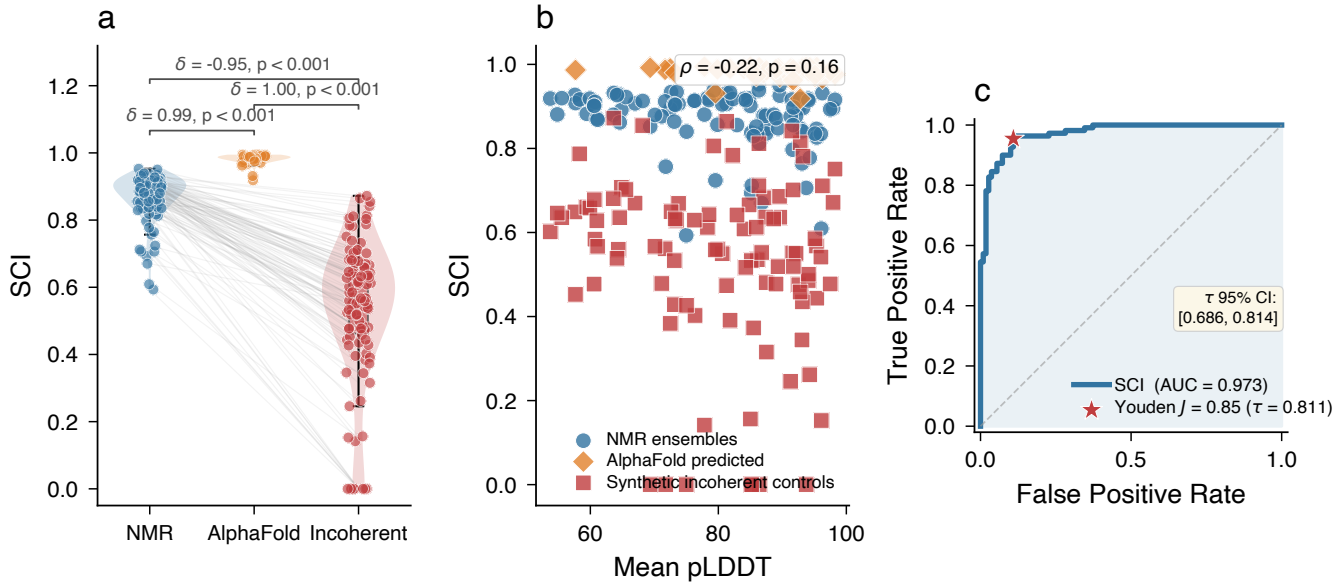


Fig. 2. Main results. (a) SCI distribution across the Main110 NMR cohort, matched synthetic incoherent controls, and 40 AlphaFold single-structure proxies. Brackets indicate pairwise Cliff's δ and corrected p -values. (b) SCI versus mean pLDDT for the AlphaFold reference structures, showing a weak non-significant association. (c) ROC curve for the grouped primary Main110 task (AUC = 0.973); the star marks the Youden- J operating point ($\tau = 0.811$).

TABLE II
STATISTICAL SUMMARY FOR THE MAIN110 MANUSCRIPT.

Test	Statistic	Value	Note
<i>Primary discrimination: grouped Main110</i>			
Paired permutation	p	$< 10^{-4}$	$n = 10,000$ permutations
AUC-ROC	—	0.9726	SCI as score
Cliff's δ	δ	-0.945	higher SCI in NMR ensembles
Paired difference	mean	0.337	95% CI: [0.305, 0.370]
Youden's J	τ^*	0.811	sens. 95.5%, spec. 89.1%
Threshold 95% CI	—	[0.686, 0.814]	bootstrap
<i>Sensitivity and holdout confirmation</i>			
PDB-level sensitivity	AUC-ROC	0.9716	$\delta = -0.943, \tau^* = 0.813$
Independent holdout	AUC-ROC	0.9835	$\delta = -0.967, \tau^* = 0.866$
<i>Reference-only three-group comparison</i>			
Kruskal-Wallis	H	205.52	$p = 2.36 \times 10^{-45}$
Mann-Whitney (NMR vs. incoherent control)	U	11769.0	$p_{\text{corr}} = 2.67 \times 10^{-33}$
Mann-Whitney (NMR vs. AF)	U	29.0	$p_{\text{corr}} = 8.56 \times 10^{-20}$
Mann-Whitney (control vs. AF)	U	0.0	$p_{\text{corr}} = 2.67 \times 10^{-20}$

$-0.224, p = 0.165$). We therefore retain AlphaFold only as a sanity check on the spectral machinery and not as mechanistic evidence about prediction confidence.

C. Effective Rank and Eigenvalue Diagnostics

Table V and Fig. 3 show that the expanded cohort preserves the same spectral signature seen in the pilot study: experimental ensembles have much lower effective rank and much more

concentrated eigenspectra than synthetic incoherent controls. Main110 NMR ensembles had mean $r_{\text{eff}} = 2.13 \pm 0.67$ versus 7.93 ± 2.59 for controls, with mean top-1 energy fractions of 0.695 and 0.340 and mean top-3 fractions of 0.850 and 0.481, respectively. In other words, coherent NMR variability continues to be driven by a few dominant distance-space modes, whereas synthetic incoherent controls distribute variance across many more directions.

The figure also shows that the effective-rank result is not

TABLE III

FUNCTION-CLASS SUMMARY FOR THE GROUPED MAIN110 COHORT. MEAN SCI AND MEAN σ_{R_g} ARE REPORTED FOR THE NMR SIDE OF EACH ANALYSIS GROUP, TOGETHER WITH LEAVE-ONE-FUNCTION-CLASS-OUT (LOFO) AUC FOR SCI AND σ_{R_g} AND THE NUMBER OF THRESHOLD-FAILED NMR GROUPS AND THRESHOLD-EXCEEDING SYNTHETIC INCOHERENT CONTROLS.

Function class	n groups	Mean SCI	Mean σ_{R_g} (Å)	SCI LOFO	σ_{R_g} LOFO	NMR $< \tau$	Control $> \tau$
chaperone	3	0.824	0.292	1.000	1.000	1	0
other	6	0.830	0.390	0.944	1.000	1	1
toxin	5	0.843	0.106	0.960	1.000	1	0
enzyme	22	0.850	0.484	0.983	0.977	3	0
transport	13	0.854	0.624	0.964	0.988	3	0
viral	8	0.858	0.189	0.906	0.984	1	1
immune	9	0.870	0.206	0.963	0.938	1	2
signaling	15	0.889	0.441	0.996	0.987	1	1
idp	7	0.894	0.393	0.959	0.980	0	1
structural	9	0.899	2.188	1.000	1.000	0	0
dna_rna_binding	13	0.911	1.472	1.000	1.000	0	0

TABLE IV

REPRESENTATIVE LOW-MARGIN AND THRESHOLD-SENSITIVE MAIN110 GROUPS. Δ SCI DENOTES THE DIVERSE-MINUS-CONTROL SCI MARGIN WITHIN EACH MATCHED GROUP.

PDB	Function class	L	M	Δ SCI	Error pattern
2KUX	other	30	20	0.033	control above τ , $L \leq 50$
2MCR	immune	36	30	0.059	control above τ , $L \leq 50$
1SKH	idp	30	22	0.060	control above τ , $L \leq 50$
7OFO	viral	30	20	0.066	control above τ , $L \leq 50$
5LBJ	signaling	35	20	0.075	control above τ , $L \leq 50$
6QES	immune	40	10	0.118	NMR below τ , $M \leq 10$, $L \leq 50$
2LM3	enzyme	205	10	0.694	NMR below τ , $M \leq 10$
1Q5F	other	156	10	0.593	NMR below τ , $M \leq 10$

TABLE V
EFFECTIVE-RANK SUMMARY BY GROUP.

Group	r_{eff}	Top-1 frac.	Top-3 frac.
Main110 NMR	2.13 ± 0.67	0.695	0.850
Synthetic incoherent controls	7.93 ± 2.59	0.340	0.481
AlphaFold proxy	2.20 ± 0.44	—	—

tied to a single formula. Participation-ratio SCI and entropy-based SCI retain near-identical orderings, so the discriminative power of the metric is coming primarily from the distance-variance representation rather than from one specific spectrum summary.

These results also explain why SCI softens on Main110 without implying that the spectral signal itself is weak. When we benchmark raw spectral quantities directly, r_{eff} , the top-1 energy fraction, and the top-3 energy fraction all reach grouped and leave-one-function-class-out AUCs near 0.99, with perfect holdout discrimination (Table VI). Likewise, augmenting SCI with residue count and model count lifts grouped CV AUC from 0.968 to 0.996. We treat these rescue models as explanatory rather than as replacements for SCI: they show that the main performance loss on Main110 is driven by the bounded normalization across heterogeneous L and M , not by disappearance of the underlying spectral separation. We do not recommend r_{eff} or top-energy fractions as primary practical QC scores because, unlike SCI, they do not provide a shared $[0, 1]$ -bounded scale and require recalibration across proteins with different residue counts and ensemble sizes. SCI therefore trades some discrimination for a portable, interpretable coherence summary that can be compared across heterogeneous cohorts on a common scale.

D. Comparison with Baseline Metrics

The expanded cohort changes the comparative ranking of metrics. At the single-metric raw-discrimination level, SCI remained strong (AUC = 0.9726), σ_{R_g} was higher (AUC = 0.9859), PCA variance ratio remained competitive (AUC = 0.9669), and contact density stayed near chance (AUC = 0.5051). However, Main110 makes the relative positioning more explicit than the pilot: across every reported regime, σ_{R_g} is the stronger single-feature discriminator, and the multifeature QC-full model is strongest overall. We therefore do not claim that SCI is the empirically best scalar on this benchmark.

Table VII therefore summarizes the current predictive comparison. SCI remained robust under grouped stratified cross-validation and leave-one-function-class-out testing (AUC = 0.9681 and 0.9707), confirming that the coherence signal generalizes beyond individual proteins. Yet the best-performing predictive model on the expanded cohort was QC-full, which combines SCI, σ_{R_g} , PCA variance ratio, and smoothness (AUC = 0.9893 grouped CV; 0.9896 leave-one-function-class-out). This shift in ranking is informative. It shows that SCI should be interpreted as the most transparent coherence axis, not as a claim to dominate amplitude-sensitive baselines on every discrimination task. Amplitude and plausibility features carry additional information once the benchmark is scaled to Main110. Figure 4 visualizes the same ranking at the level of the manuscript’s three transfer-oriented validation regimes.

E. Robustness Analysis

1) *Noise Sweep*: SCI classification performance remained nearly invariant across all tested noise levels used in synthetic incoherent control generation ($\sigma = 0.05$ – 0.50 Å): AUC-ROC

TABLE VI
SPECTRAL RESCUE ANALYSIS. THESE MODELS ARE REPORTED TO EXPLAIN WHY SCI SOFTENS ON MAIN110; THEY DO NOT REPLACE SCI AS THE CANONICAL HEADLINE METRIC.

Model	Raw AUC	Grouped CV AUC	LOFO AUC	Holdout AUC
SCI	0.973	0.968	0.971	0.983
r_{eff}	0.991	0.990	0.990	1.000
Top-1 energy fraction	0.992	0.990	0.990	1.000
Top-3 energy fraction	0.992	0.991	0.991	1.000
SCI + n_{models}	0.987	0.984	0.985	1.000
SCI + n_{residues}	0.986	0.983	0.984	0.975
SCI + n_{residues} + n_{models}	0.998	0.996	0.997	1.000

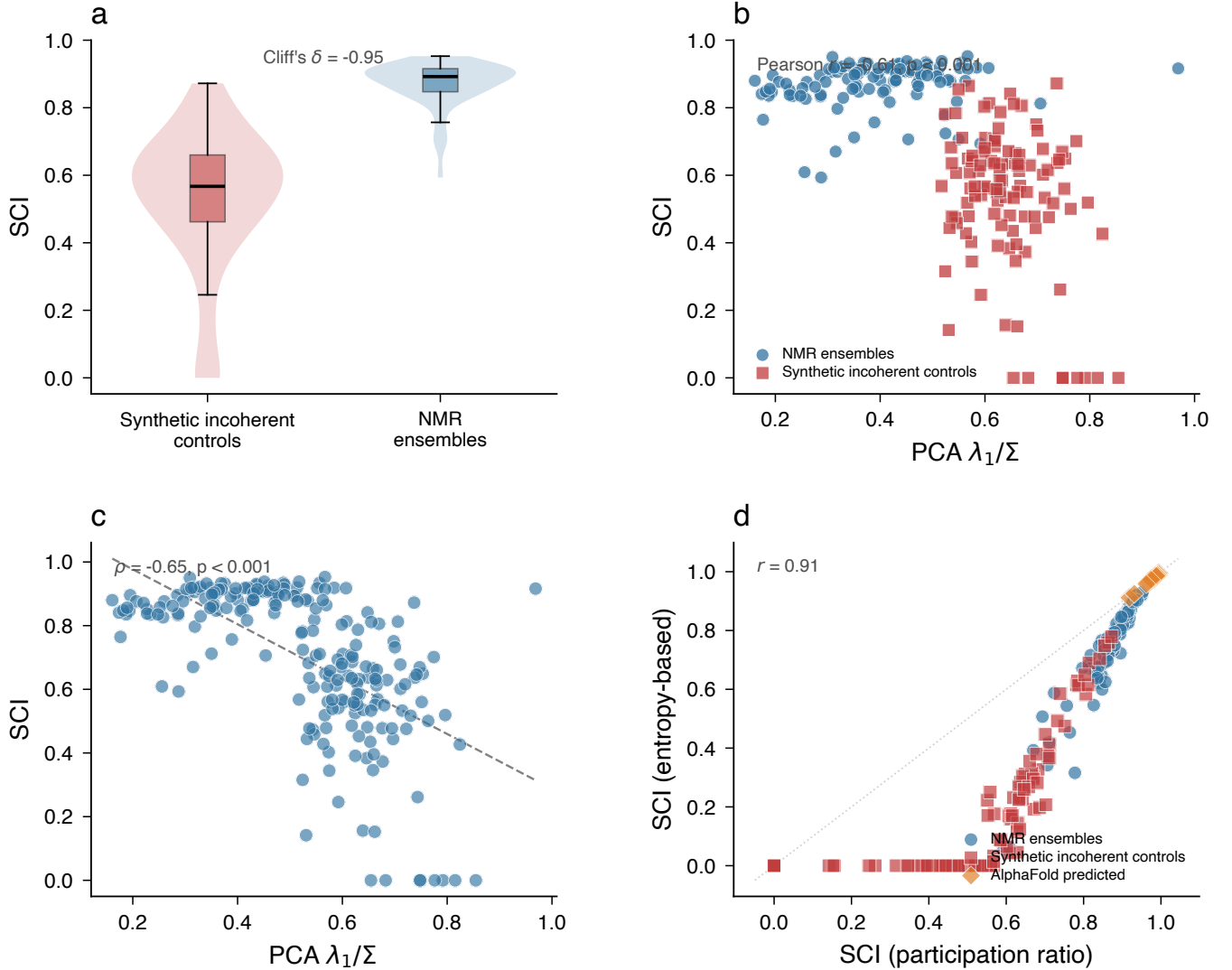


Fig. 3. Spectral diagnostics. (a) SCI distribution for Main110 NMR ensembles versus matched synthetic incoherent controls. (b) SCI versus PCA first-component variance ratio. (c) Rank-correlation between SCI and PCA variance ratio. (d) Participation-ratio SCI versus entropy-based SCI, illustrating that the main ranking is driven by the distance-variance representation rather than the specific effective-rank formula.

ranged from 0.9716 to 0.9728, and Cliff's δ from -0.9431 to -0.9456 (Table VIII; Fig. 5). The 95% bootstrap CI for the mean paired difference narrowed only slightly across the sweep, consistent with a very modest reduction in the NMR-control gap as the synthetic incoherent controls gain variance. The headline SCI separation therefore does not rest on a narrow perturbation setting.

2) *Youden's J Threshold and Contact-Threshold Sensitivity*: Youden's- J thresholding identifies a practical operating point for the grouped primary analysis, but the expanded cohort shows that thresholds should be interpreted as screening heuristics rather than universal pass/fail rules. The grouped Main110 optimum was $\tau^* = 0.811$ with 95.5% sensitivity and 89.1% specificity, while the PDB-level sensitivity

TABLE VII
BASELINE AND MULTIMETRIC COMPARISON ON THE EXPANDED COHORT.

Metric or model	Raw AUC	Grouped CV AUC	LOFO AUC	Holdout AUC	Direction
SCI	0.9726	0.9681	0.9707	0.9835	higher → NMR
σ_{R_g}	0.9859	0.9860	0.9803	1.0000	higher → NMR
PCA λ_1/Σ	0.9669	—	—	—	higher → control
Contact density	0.5051	—	—	—	uninformative
SCI + σ_{R_g}	0.9837	0.9725	0.9742	1.0000	multivariate
QC-full	0.9929	0.9893	0.9896	1.0000	multivariate

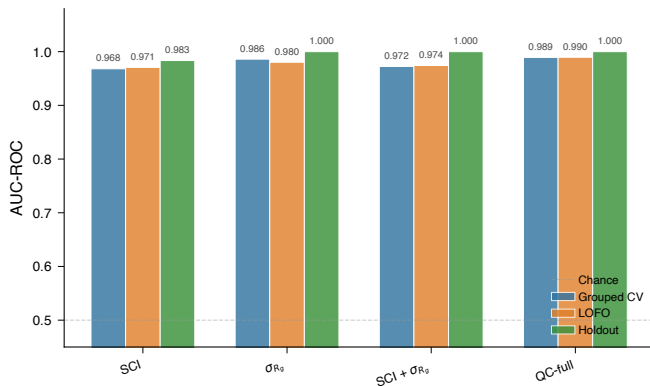


Fig. 4. Baseline metric comparison. The current manuscript emphasizes grouped CV, leave-one-function-class-out, and independent holdout performance for SCI, σ_{R_g} , SCI+ σ_{R_g} , and QC-full.

TABLE VIII
NOISE SWEEP: SCI DISCRIMINATION ACROSS
SYNTHETIC-INCOHERENT-CONTROL NOISE LEVELS.

σ (Å)	AUC	δ	95% CI (paired Δ)	p
0.05	0.9728	-0.9456	[0.306, 0.371]	$< 10^{-4}$
0.10	0.9727	-0.9455	[0.305, 0.371]	$< 10^{-4}$
0.20	0.9726	-0.9453	[0.305, 0.370]	$< 10^{-4}$
0.30	0.9726	-0.9451	[0.304, 0.369]	$< 10^{-4}$
0.50	0.9716	-0.9431	[0.301, 0.367]	$< 10^{-4}$

analysis yielded a closely matching optimum ($\tau^* = 0.813$). The contact-based SCI variant retained qualitative separation between NMR and synthetic incoherent ensembles across multiple contact cutoffs, but its exact values shifted with threshold choice, reinforcing why the manuscript anchors its claims on the continuous distance-based formulation.

3) *Ensemble-Size Sensitivity*: Subsampling analysis shows that SCI stability depends strongly on the number of available conformers. The mean absolute deviation from the full-ensemble SCI estimate shrank from 0.548 at five models to 0.154 at ten, 0.050 at fifteen, and 0.005 at twenty (Table IX). This directly explains why low-model ensembles are over-represented among the Main110 NMR threshold failures and suggests that practical SCI deployment is most stable once roughly 15–20 conformers are available.

F. Exploratory: Biological Validation and Contextual Flexibility

SCI remained biologically grounded after the cohort expansion. Across 110 proteins with residue-level analyses, the median Spearman correlation between SCI-derived residue

TABLE IX
ENSEMBLE-SIZE SENSITIVITY OF SCI RELATIVE TO THE FULL-ENSEMBLE ESTIMATE.

Models retained	Mean abs. deviation	Median abs. deviation	n
5	0.548	0.515	790
10	0.154	0.135	790
15	0.050	0.043	790
20	0.005	0.000	790

contributions and experimental RMSF was 0.587, while the median correlation between GNM-predicted and experimental RMSF was 0.701. In 108 of the 110 proteins, residue contributions were positively associated with RMSF. A paired Wilcoxon comparison rejected equality in the direction GNM $>$ contribution (one-sided $p = 0.0189$; two-sided $p = 0.0378$), indicating that the SCI-derived contribution map is biologically meaningful but does not replace a structure-based elasticity model.

The residue-level outliers are informative (Table X). Only two proteins showed negative contribution-versus-RMSF associations (1ARK and 1YS5), and three additional proteins remained weak ($\rho < 0.2$): 1OQY, 2JQF, and 6U1O. None of these five overlap the grouped SCI threshold-failed set. The threshold-failed protein 2LM3, by contrast, still showed a positive residue-level correlation ($\rho = 0.213$), indicating that ensemble-level screening errors and residue-level biological outliers are not the same phenomenon. The two negative cases point to different failure modes. For 1ARK, both SCI contribution and GNM are weak, suggesting a flexibility pattern that is not well captured by either a low-rank SCI contribution map or a simple elastic-network description. For 1YS5, GNM remains moderately aligned with RMSF whereas SCI contribution is nearly flat, indicating that the residue-level SCI map and GNM are emphasizing different aspects of the underlying motion.

The pair-based analyses are therefore best interpreted as contextual case studies rather than as formal validation layers. Across 14 allosteric pairs, the median absolute change in SCI-derived summary was only 0.00356, whereas the corresponding median absolute changes were 0.208 for contact density and 4.276 Å for radius of gyration. Across 3 apo/holo pairs, the same pattern persisted (median absolute changes 0.000319, 0.0582, and 0.831 Å, respectively), but the sample is too small to support formal inference. The 4 available intrinsically disordered proteins remained highly flexible (median mean RMSF 1.878 Å) while still showing high single-structure proxy SCI (median 0.974), reinforcing that coherence and flexibility are not the same biological dimension.

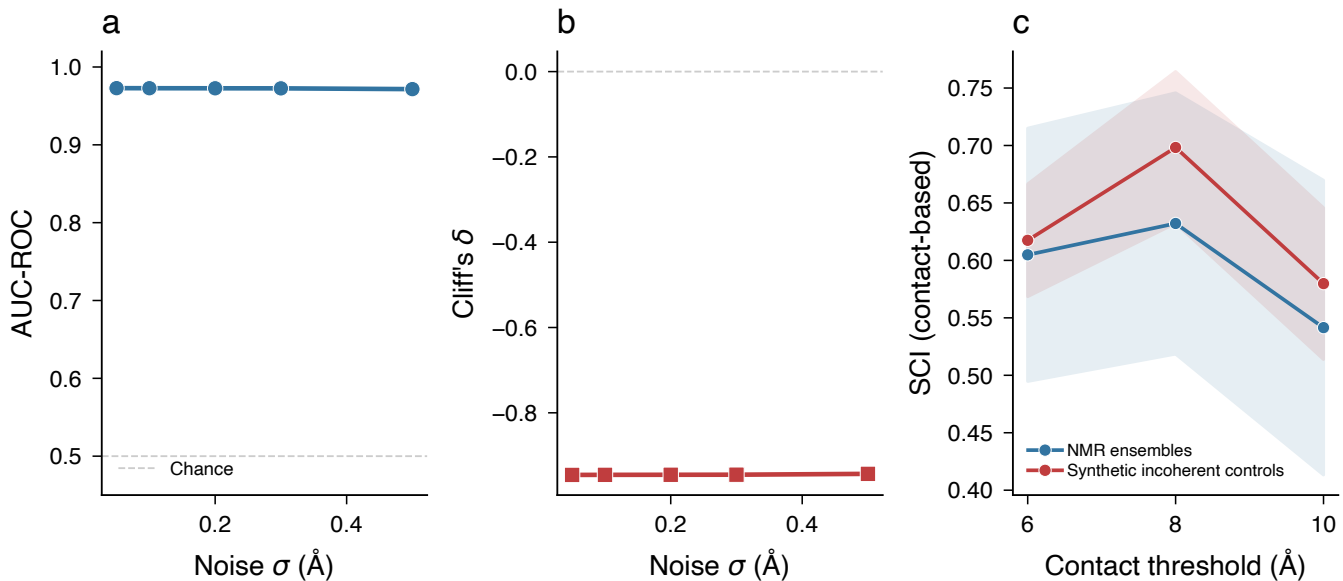


Fig. 5. Robustness analysis. (a) AUC-ROC versus injected noise level. (b) Cliff's δ versus injected noise. (c) Contact-based SCI versus contact threshold across NMR, matched synthetic incoherent controls, and AlphaFold references.

TABLE X
LOWEST RESIDUE-LEVEL SCI CONTRIBUTION CORRELATIONS WITH
EXPERIMENTAL RMSF.

PDB	L	Contribution vs. RMSF	GNM vs. RMSF	Note
1ARK	60	-0.505	0.125	negative
1YS5	156	-0.025	0.493	negative
1QY	363	0.056	-0.632	weak
2JQF	166	0.081	0.239	weak
6U10	258	0.110	-0.329	weak

G. Eigenvector Smoothness as a Complementary Diagnostic

Having established that coherence and amplitude form the two primary QC axes, we asked whether a complementary spatial-plausibility attribute adds information not captured by either. The mean top-eigenvector smoothness score was 0.916 ± 0.070 for NMR versus 0.842 ± 0.027 for synthetic incoherent controls, with a moderate-to-large effect size (Cliff's $\delta = -0.678$) and paired permutation $p < 10^{-4}$. AlphaFold proxy values were highest (0.963 ± 0.035), consistent with single structures producing very smooth dominant geometric modes.

Among the Main110 NMR ensembles, smoothness was positively correlated with SCI (Spearman $\rho = 0.365$, $p < 10^{-4}$) but even more strongly with σ_{R_g} ($\rho = 0.833$, $p \ll 10^{-6}$), suggesting that it captures partially independent information while remaining closer to a plausibility check than to a primary discrimination axis. The $\text{SCI} \times \sigma_{R_g}$ map and the smoothness overlays therefore provide a useful multimetric QC representation, but not a single universal decision rule.

H. Failure Mode Analysis

The four synthetic stress tests occupy distinct regions of the $\text{SCI} \times \sigma_{R_g}$ plane and therefore remain useful for interpreting which metric is carrying each detection decision. Gaussian

TABLE XI
FAILURE MODE DETECTION RATES. INDIVIDUAL METRIC DETECTION
RATES (PERCENTAGE OF ENSEMBLES FLAGGED) AND COMBINED QC GATE
PERFORMANCE ACROSS FOUR SYNTHETIC FAILURE TYPES.
EXPANDED-COHORT NMR FALSE-POSITIVE RATE UNDER THE FIXED
COMBINED THRESHOLDS: 10.1%.

Failure type	SCI	σ_{R_g}	Smooth.	Combined
i.i.d. Gaussian	14%	96%	0%	96%
Mode collapse	85%	96%	0%	97%
Residue shuffle	16%	100%	0%	100%
High-rank ($K = 10$)	41%	97%	0%	97%

and residue-shuffle artifacts tend to preserve deceptively high SCI while collapsing amplitude, whereas mode-collapse and high-rank perturbation reduce SCI more strongly. This pattern is why σ_{R_g} and SCI remain complementary even after the expanded cohort analysis shows that amplitude-aware models can outperform SCI on some generalization benchmarks. Table XI and Fig. 7 summarize these failure-type-specific detection patterns.

V. DISCUSSION

A. Methodological Advantages of SCI

The central contribution of this manuscript is not a new mathematical definition relative to the internal 27-protein pilot, but a more demanding validation setting. Main110 shows that the pilot signal survives broader heterogeneity, while also revealing softer specificity, function-class variation, and threshold non-transferability that were invisible at pilot scale. Those findings are scientifically useful because they clarify where SCI is robust on its own and where complementary QC axes become necessary.

Within that broader setting, SCI still offers several methodological advantages over existing ensemble-diversity measures. First, it is *rotation-invariant*: because SCI operates

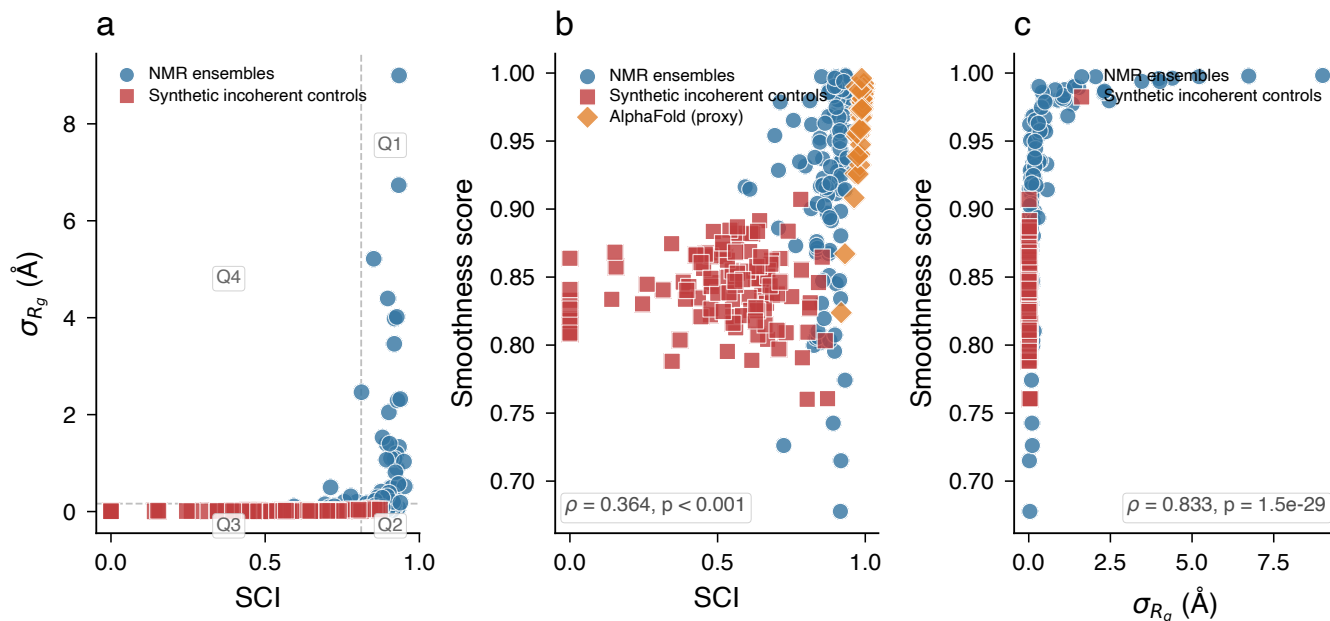


Fig. 6. Multi-metric QC diagnostics. (a) SCI versus σ_{R_g} for all samples. (b) Top-eigenvector smoothness score versus SCI. (c) Smoothness versus σ_{R_g} . The weak-to-moderate SCI–smoothness correlation indicates partially independent diagnostic axes.

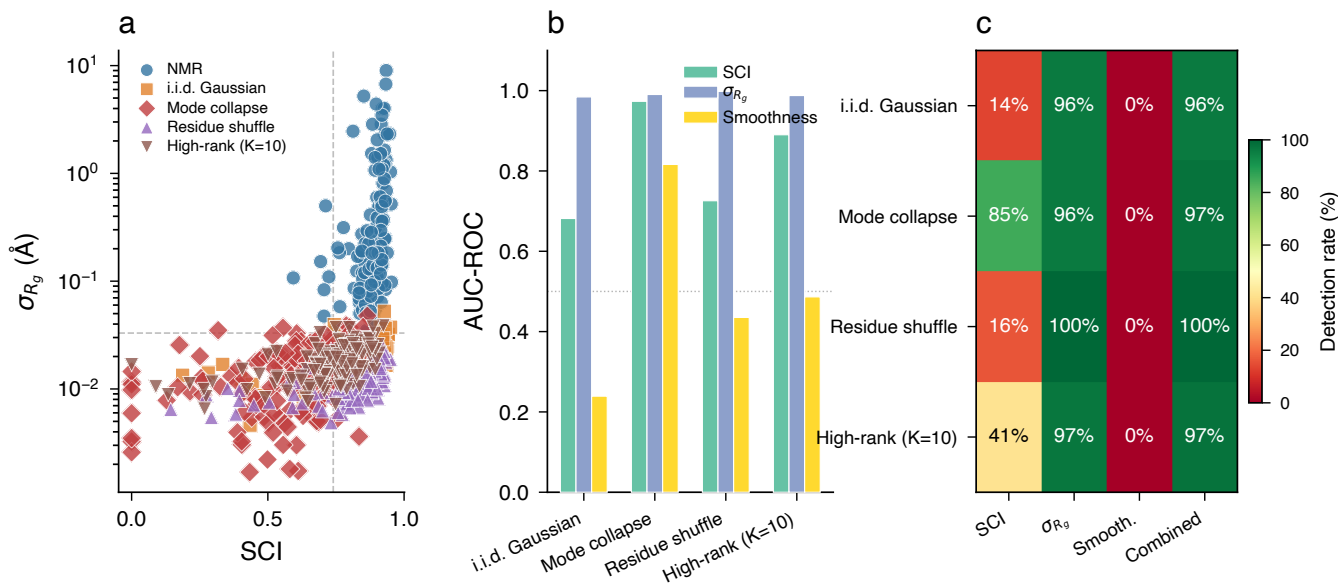


Fig. 7. Failure mode analysis for the expanded QC stress tests. (a) SCI versus σ_{R_g} for NMR ensembles and four synthetic artifact classes, with dashed screening thresholds. (b) AUC-ROC per metric per failure type. (c) Detection rate heatmap showing individual-metric and combined screening performance.

on pairwise distances rather than Cartesian coordinates, no structural superposition or reference frame is required. This eliminates a well-known source of bias in PCA-based metrics and RMSD calculations [11], [12]. Second, SCI is *model-free*: it requires no force field, energy function, or normal-mode computation. Third, SCI produces a *single number* on $[0, 1]$ with a direct spectral interpretation, providing a bounded, portable comparison scale across heterogeneous ensembles even though that normalization can cost some discrimination in broader cohorts. Fourth, SCI is *sensitive to local coordinated*

motions in principle: unlike σ_{R_g} , which captures only global size fluctuations, SCI can detect coordinated loop rearrangements, domain twists, and hinge motions that leave overall size weakly changed.

B. Physical Interpretation of SCI Direction

A key insight from the Main110 results is the relationship between coordinate-space and distance-space complexity. Low-rank deformations in coordinate space do not automatically produce low-rank structure in distance-variance space,

because the nonlinear distance function $D(i, j) = \|\mathbf{r}_i - \mathbf{r}_j\|$ introduces cross-terms that disperse variance across many eigenvalues. Conversely, coordinated conformational motions such as hinge bending and domain closure produce highly correlated distance changes across many residue pairs, concentrating the distance-variance spectrum into a few dominant modes. High SCI should therefore be interpreted as *high motion coherence*, not simply as low dimensionality or low structural variability. The rescue analyses summarized in Table VI sharpen this interpretation. Raw spectral summaries such as r_{eff} and the top-energy fractions remain near 0.99 AUC on Main110, whereas normalized SCI softens to 0.973. Likewise, adding n_{residues} and n_{models} to SCI nearly restores perfect discrimination. The most parsimonious explanation is that Main110 heterogeneity enters mainly through the bounded normalization $d = \min(L, M-1)$: as protein length and model count vary more widely, the same underlying spectral concentration is compressed unevenly. We therefore view the current SCI as an interpretable normalized score: a bounded, portable coherence summary whose shared scale facilitates cross-protein comparison, even though that portability carries a measurable discrimination tradeoff on heterogeneous cohorts. The rescue models indicate that the underlying spectral signal remains stronger than the headline SCI alone suggests.

C. Limitations

Several limitations should be noted. First, although Main110 is substantially larger than the pilot cohort, it is still modest relative to the full diversity of NMR structures in the PDB, and the fixed holdout contains only 11 proteins. Moreover, the holdout spans only 27–75 residues, which samples the small-protein end of the main-cohort size range and therefore does not directly test external transfer for large proteins ($L > 100$). Second, the AlphaFold analysis uses a single-structure proxy that measures fold-geometry concentration rather than cross-conformer coherence; the weak pLDDT association reinforces that this result should be interpreted only as a reference comparison. Third, the synthetic incoherent controls and failure-mode generators do not span all real-world failure cases. In particular, the expanded cohort shows that fixed thresholds calibrated on synthetic artifacts produce a non-negligible NMR false-positive rate (10.1%), so they should be treated as screening heuristics rather than universal accept/reject rules. Fourth, the pair-based allosteric and apo/holo analyses are descriptive rather than inferential because the available sample sizes are small. Fifth, this manuscript deliberately leaves molecular-dynamics benchmarking out of scope; future work should test SCI on MD trajectories, AlphaFold-derived ensembles, and poorly converged experimental refinements.

D. Practical Guidance: When SCI Is and Is Not Informative

SCI measures spectral concentration of the distance-variance matrix. It is most informative when comparing ensembles generated by the same or closely related procedures, where a substantially lower SCI flags incoherent or insufficiently converged variation. The Main110 results also make clear, however, that SCI should not be treated as a complete

Procedure: Three-Metric Ensemble QC Gate

Input: Ensemble $\{S_1, \dots, S_M\}$ with C α coordinates.

Output: QC summary in terms of coherence, amplitude, and plausibility.

Step 1. Compute $V(i, j) = \text{Var}_m[D_m(i, j)]$ and derive SCI via Eq. (7).

Step 2. Compute σ_{R_g} across models.

Step 3. Compute top-eigenvector smoothness via the Rayleigh quotient on \mathcal{L} (Section III-D).

Step 4. Report the ensemble on the SCI \times σ_{R_g} plane and use smoothness as a supporting plausibility check.

Interpretation: Fixed thresholds such as $\tau_{\text{SCI}} = 0.74$, $\tau_{\sigma_{R_g}} = 0.033$ Å, and $\tau_{\text{smooth}} = 0.75$ are useful screening heuristics for the synthetic stress tests, but on Main110 they still flag 10.1% of the NMR reference set. They should therefore be used for triage rather than as universal pass/fail rules.

Fig. 8. Recommended QC procedure. SCI and σ_{R_g} define the core 2D detection plane, while smoothness adds a spatial plausibility check. The fixed thresholds summarize the synthetic stress tests but are not universal acceptance criteria on Main110.

one-number surrogate for ensemble quality. σ_{R_g} is the empirically stronger single-feature discriminator on this benchmark, and QC-full is strongest overall. Synthetic artifacts such as i.i.d. Gaussian noise can also retain moderately high SCI despite lacking physically meaningful structural coordination.

We therefore recommend reporting three complementary quantities:

- 1) **SCI** as the core coherence axis and the most interpretable summary of whether variation is organized into a few coordinated modes.
- 2) σ_{R_g} as an amplitude axis that catches low-variation artifacts and, on Main110, provides the strongest standalone discrimination.
- 3) **Smoothness score** as a spatial plausibility check on the dominant mode.

Table IX shows that the mean absolute SCI deviation from the full-ensemble estimate shrank from 0.548 at five models to 0.154 at ten, 0.050 at fifteen, and 0.005 at twenty, suggesting that SCI is most stable once roughly 15–20 conformers are available. Fig. 8 summarizes the recommended practical workflow.

E. Informatics Relevance

SCI is not intended to explain dynamical mechanisms but to serve as an automated informatics QC metric for large-scale structural resources and ensemble-generation pipelines. When ensemble quality is unchecked, downstream biomedical inferences such as binding-site prediction, epitope mapping, and variant interpretation may silently propagate artifacts from incoherent ensembles. The Main110 results suggest that SCI is most useful when reported with grouped inference, a PDB-level sensitivity check, and complementary amplitude and smoothness diagnostics.

F. Future Directions

Several extensions are natural. SCI could be applied to molecular dynamics trajectories by treating snapshots as en-

semble members, enabling coherence-aware quality assessment of conformational sampling. The same framework could be used to compare experimentally derived NMR ensembles with ensemble-generating predictors such as AF-Cluster or Boltzmann-style models [47], [48]. At the residue level, the current biological validation motivates closer integration of SCI-derived contribution maps with allostery analysis, disorder characterization, and function-specific classifiers.

VI. CONCLUSION

We have proposed the Spectral Coherence Index (SCI), a model-free, rotation-invariant metric for quantifying how coherently conformational variation is organized in protein structural ensembles. On the expanded Main110 cohort, SCI robustly separates experimental NMR ensembles from matched synthetic incoherent controls at the grouped primary level (AUC = 0.9726, Cliff's $\delta = -0.945$), remains stable at the PDB level (AUC = 0.9716), and transfers to an independent 11-protein holdout (AUC = 0.9835).

The expanded benchmark clarifies the role of SCI in a modern ensemble-QC stack. σ_{R_g} is the stronger empirical single-feature discriminator on Main110, while SCI remains the most interpretable single coherence signal, with strong grouped and leave-one-function-class-out generalization. Rescue analyses show that the underlying spectral separation remains very strong and that much of the observed softening comes from normalization across heterogeneous residue counts and model counts rather than from loss of the spectral signal itself. A QC-augmented model achieves the best predictive performance by combining SCI with amplitude and plausibility features. Residue-level biological validation links SCI-derived contributions to experimental RMSF and GNM predictions, and the AlphaFold reference analysis supports the spectral formalism while emphasizing that single-structure proxies are not substitutes for ensemble coherence.

Overall, SCI should be viewed as a principled coherence axis for protein-ensemble informatics: not the empirically strongest standalone discriminator on Main110, but the most transparent bounded summary of coherent distance-space organization. Its practical value lies in providing a portable comparison scale across heterogeneous ensembles, even when that portability entails a measurable discrimination tradeoff, and it is therefore most useful when embedded in grouped evaluation and a multi-metric QC workflow.

REFERENCES

- [1] K. A. Henzler-Wildman and D. Kern, "Dynamic personalities of proteins," *Nature*, vol. 450, no. 7172, pp. 964–972, Dec. 2007.
- [2] H. Frauenfelder, S. G. Sligar, and P. G. Wolynes, "The energy landscapes and motions of proteins," *Science*, vol. 254, no. 5038, pp. 1598–1603, Dec. 1991.
- [3] A. M. J. J. Bonvin, R. Boelens, and R. Kaptein, "NMR analysis of protein interactions," *Curr. Opin. Chem. Biol.*, vol. 9, no. 5, pp. 501–508, 2005.
- [4] G. M. Clore and C. D. Schwieters, "How much backbone motion in ubiquitin is required to account for dipolar coupling data measured in multiple alignment media as assessed by independent cross-validation?" *J. Am. Chem. Soc.*, vol. 126, no. 9, pp. 2923–2938, 2004.
- [5] G. T. Montelione *et al.*, "Recommendations of the wwPDB NMR validation task force," *Structure*, vol. 21, no. 9, pp. 1563–1570, Sep. 2013.
- [6] J. Jumper *et al.*, "Highly accurate protein structure prediction with AlphaFold," *Nature*, vol. 596, no. 7873, pp. 583–589, Aug. 2021.
- [7] M. Baek *et al.*, "Accurate prediction of protein structures and interactions using a three-track neural network," *Science*, vol. 373, no. 6557, pp. 871–876, Aug. 2021.
- [8] Z. Lin *et al.*, "Evolutionary-scale prediction of atomic-level protein structure with a language model," *Science*, vol. 379, no. 6637, pp. 1123–1130, Mar. 2023.
- [9] D. del Alamo, D. Sala, H. S. Bhatt, T. Lehmann, and J. Meiler, "Sampling alternative conformational states of transporters and receptors with AlphaFold2," *eLife*, vol. 11, Art. no. e75751, Mar. 2022.
- [10] B. Jing *et al.*, "AlphaFold meets flow matching for generating protein ensembles," in *Proc. Int. Conf. Mach. Learn. (ICML)*, 2024, pp. 22031–22043.
- [11] R. Diamond, "On the use of normal modes in thermal parameter refinement: Theory and application to the bovine pancreatic trypsin inhibitor," *Acta Crystallogr. D*, vol. 46, no. 5, pp. 425–435, 1990.
- [12] I. Kufareva and R. Abagyan, "Methods of protein structure comparison," in *Homology Modeling: Methods and Protocols*. New York, NY, USA: Humana Press, 2012, pp. 231–257.
- [13] M. Y. Lobanov, N. S. Bogatyreva, and O. V. Galzitskaya, "Radius of gyration as an indicator of protein structure compactness," *Mol. Biol.*, vol. 42, no. 4, pp. 623–628, 2008.
- [14] A. Amadei, A. B. M. Linssen, and H. J. C. Berendsen, "Essential dynamics of proteins," *Proteins*, vol. 17, no. 4, pp. 412–425, Dec. 1993.
- [15] C. C. David and D. J. Jacobs, "Principal component analysis: A method for determining the essential dynamics of proteins," in *Protein Dynamics: Methods and Protocols*. New York, NY, USA: Humana Press, 2014, pp. 193–226.
- [16] M. Vendruscolo, E. Paci, C. M. Dobson, and M. Karplus, "Three key residues form a critical contact network in a protein folding transition state," *Nature*, vol. 409, no. 6820, pp. 641–645, 2001.
- [17] W. Li and A. Godzik, "Cd-hit: A fast program for clustering and comparing large sets of protein or nucleotide sequences," *Bioinformatics*, vol. 22, no. 13, pp. 1658–1659, Jul. 2006.
- [18] I. Bahar, A. R. Atilgan, and B. Erman, "Direct evaluation of thermal fluctuations in proteins using a single-parameter harmonic potential," *Fold. Des.*, vol. 2, no. 3, pp. 173–181, 1997.
- [19] T. Haliloglu, I. Bahar, and B. Erman, "Gaussian dynamics of folded proteins," *Phys. Rev. Lett.*, vol. 79, no. 16, pp. 3090–3093, Oct. 1997.
- [20] A. R. Atilgan, S. R. Durell, R. L. Jernigan, M. C. Demirel, O. Keskin, and I. Bahar, "Anisotropy of fluctuation dynamics of proteins with an elastic network model," *Biophys. J.*, vol. 80, no. 1, pp. 505–515, Jan. 2001.
- [21] O. Roy and M. Vetterli, "The effective rank: A measure of effective dimensionality," in *Proc. 15th Eur. Signal Process. Conf. (EUSIPCO)*, Poznan, Poland, 2007, pp. 606–610.
- [22] R. Vershynin, *High-Dimensional Probability: An Introduction with Applications in Data Science*. Cambridge, U.K.: Cambridge Univ. Press, 2018.
- [23] M. Scheurer, A. Dreuw, E. Schwab, and M. Bhatt, "Exploration of conformational landscapes using spectral entropy," *J. Chem. Theory Comput.*, vol. 11, no. 12, pp. 5543–5553, 2015.
- [24] A. E. Garcia, "Large-amplitude nonlinear motions in proteins," *Phys. Rev. Lett.*, vol. 68, no. 17, pp. 2696–2699, Apr. 1992.
- [25] M. A. Balseira, W. Wriggers, Y. Oono, and K. Schulten, "Principal component analysis and long time protein dynamics," *J. Phys. Chem.*, vol. 100, no. 7, pp. 2567–2572, 1996.
- [26] A. Rives *et al.*, "Biological structure and function emerge from scaling unsupervised learning to 250 million protein sequences," *Proc. Natl. Acad. Sci. U.S.A.*, vol. 118, no. 15, Art. no. e2016239118, Apr. 2021.
- [27] G. Ahdriz *et al.*, "OpenFold: Retraining AlphaFold2 yields new insights into its learning mechanisms and capacity for generalization," *Nature Methods*, vol. 21, no. 8, pp. 1514–1524, Aug. 2024.
- [28] D. E. Shaw *et al.*, "Atomic-level characterization of the structural dynamics of proteins," *Science*, vol. 330, no. 6002, pp. 341–346, Oct. 2010.
- [29] S. A. Hollingsworth and R. O. Dror, "Molecular dynamics simulation for all," *Neuron*, vol. 99, no. 6, pp. 1129–1143, Sep. 2018.
- [30] R. B. Best, K. Lindorff-Larsen, M. A. DePristo, and M. Vendruscolo, "Relation between native ensembles and experimental structures of proteins," *Proc. Natl. Acad. Sci. U.S.A.*, vol. 103, no. 29, pp. 10901–10906, Jul. 2006.
- [31] Y. Zhang and J. Skolnick, "Scoring function for automated assessment of protein structure template quality," *Proteins*, vol. 57, no. 4, pp. 702–710, Dec. 2004.

- [32] A. Bhattacharya, R. Tejero, and G. T. Montelione, "Evaluating protein structures determined by structural genomics consortia," *Proteins*, vol. 66, no. 4, pp. 778–795, Mar. 2007.
- [33] K. A. Dill and J. L. MacCallum, "The protein-folding problem, 50 years on," *Science*, vol. 338, no. 6110, pp. 1042–1046, Nov. 2012.
- [34] D. D. Boehr, R. Nussinov, and P. E. Wright, "The role of dynamic conformational ensembles in biomolecular recognition," *Nature Chem. Biol.*, vol. 5, no. 11, pp. 789–796, Nov. 2009.
- [35] R. G. Smock and L. M. Gierasch, "Sending signals dynamically," *Science*, vol. 324, no. 5924, pp. 198–203, Apr. 2009.
- [36] M. Gerstein, A. M. Lesk, and C. Chothia, "Structural mechanisms for domain movements in proteins," *Biochemistry*, vol. 33, no. 22, pp. 6739–6749, 1994.
- [37] S. Hayward and H. J. C. Berendsen, "Systematic analysis of domain motions in proteins from conformational change: New results on citrate synthase and T4 lysozyme," *Proteins*, vol. 30, no. 2, pp. 144–154, 1998.
- [38] L.-W. Yang, A. J. Rader, X. Liu, C. J. Jursa, S. C. Chen, H. A. Karimi, and I. Bahar, "oGNM: Online computation of structural dynamics using the Gaussian network model," *Nucleic Acids Res.*, vol. 34, Suppl. 2, pp. W24–W31, Jul. 2006.
- [39] L.-W. Yang and I. Bahar, "Coupling between catalytic site and collective dynamics: A requirement for mechanochemical activity of enzymes," *Structure*, vol. 13, no. 6, pp. 893–904, Jun. 2005.
- [40] C. Chennubhotla and I. Bahar, "Signal propagation in proteins and relation to equilibrium fluctuations," *PLoS Comput. Biol.*, vol. 3, no. 9, Art. no. e172, Sep. 2007.
- [41] I. Borg and P. J. F. Groenen, *Modern Multidimensional Scaling: Theory and Applications*, 2nd ed. New York, NY, USA: Springer, 2005.
- [42] R. J. Bell and P. Dean, "Atomic vibrations in vitreous silica," *Discuss. Faraday Soc.*, vol. 50, pp. 55–61, 1970.
- [43] R. E. Amaro, J. Baudry, J. Chodera, O. Demir, J. A. McCammon, Y. Miao, and J. C. Smith, "Ensemble docking in drug discovery," *Biophys. J.*, vol. 114, no. 10, pp. 2271–2278, May 2018.
- [44] J. M. Thornton, M. S. Edwards, W. R. Taylor, and D. J. Barlow, "Location of 'continuous' antigenic determinants in the protruding regions of proteins," *EMBO J.*, vol. 5, no. 2, pp. 409–413, Feb. 1986.
- [45] L. Ponzoni and I. Bahar, "Structural dynamics is a determinant of the functional significance of missense variants," *Proc. Natl. Acad. Sci. U.S.A.*, vol. 115, no. 16, pp. 4164–4169, Apr. 2018.
- [46] P. Ewels, M. Magnusson, S. Lundin, and M. Källér, "MultiQC: Summarize analysis results for multiple tools and samples in a single report," *Bioinformatics*, vol. 32, no. 19, pp. 3047–3048, Oct. 2016.
- [47] R. J. L. Wayment-Steele *et al.*, "Predicting multiple conformations via sequence clustering and AlphaFold2," *Nature*, vol. 625, pp. 832–839, Jan. 2024.
- [48] F. Noé, S. Olsson, J. Köhler, and H. Wu, "Boltzmann generators: Sampling equilibrium states of many-body systems with deep learning," *Science*, vol. 365, no. 6457, eaaw1147, Sep. 2019.